ELSEVIER

Thermochimica Acta 269/270 (1995) 273–293

thermochimica acta

Thermal decomposition of phase-stabilised ammonium nitrate (PSAN), hydroxyl-terminated polybutadiene (HTPB) based propellants. The effect of iron(III) oxide burning-rate catalyst ☆

P. Carvalheira [a,*], G.M.H.J.L. Gadiot [b], W.P.C. de Klerk [b]

[a] *Departamento de Engenharia Mecânica, Faculdade de Ciências e Tecnologia da Universidade de Coimbra, Largo de D. Dinis, P-3000 Coimbra, Portugal*

[b] *TNO Prins Maurits Laboratorium, Lange Kleiweg 137, Postbus 45, 2280 AA Rijswijk, Netherlands*

Received 16 September 1994; accepted 13 March 1995

Abstract

Phase-stabilised ammonium nitrate (PSAN) and hydroxyl-terminated polybutadiene (HTPB) are the main ingredients of propellants used with success in some pyrotechnic igniter components of the VULCAIN liquid rocket engine for the ARIANE 5. Small amounts of selected additives play an important role in solving some of the problems presented by composite propellants that include ammonium nitrate (AN). Iron(III) oxide (Fe_2O_3), for example, can be used as a burning-rate modifier in PSAN/HTPB propellants and although its effect on the burning rate is well known, its mechanism of action is not well understood. Thermogravimetry (TG), differential thermogravimetry (DTG) and differential thermal analysis (DTA) have been applied to study the slow thermal decomposition of selected compositions to investigate the mechanism of action of Fe_2O_3 as a burning-rate modifier of PSAN/HTPB propellants. The compositions evaluated include PSAN, Fe_2O_3 and HTPB cross-linked with isophorone diisocyanate (IPDI) as ingredients. No effect of Fe_2O_3 on PSAN decomposition is found. Fe_2O_3 shows an effect on the kinetics of the first stage of HTPB–IPDI decomposition and increases the exothermicity of HTPB–IPDI decomposition. In the decomposition of PSAN/HTPB–IPDI/Fe_2O_3 propellants, the effect of Fe_2O_3 is also observed and a synergetic interaction between PSAN and HTPB–IPDI is found, for which a physical-chemical explanation is given.

Keywords: Catalyst; Decomposition; DTA; DTG; Propellant; TGA

* Corresponding author.

☆ Presented at the 6th European Symposium on Thermal Analysis and Calorimetry, Grado, Italy, 11–16 September 1994.

SSDI 0040-6031(95)02366-6

List of Symbols

A Arrhenius pre-exponential factor/s^{-1}
d_p particle diameter/μm
E Arrhenius activation energy/kJ mol^{-1}
f_{ox} mass fraction of oxidiser
f_b mass fraction of binder
m mass/mg
m_0 initial mass/mg
n kinetics order of reaction
p pressure/MPa
R universal gas constant/kJ mol^{-1} K^{-1}
T temperature/K
T_m temperature of sample at maximum amplitude of DTG or DTA peak/K
ΔT amplitude of DTA signal/K

Greek Symbols

α Fractional mass loss
β heating rate/K min^{-1}

1. Introduction

Interest in the kinetics of thermal decomposition of AN and HTPB partly originates from the use of these materials in gas generator propellants used for the turbo pump starter, gas generator igniter and thrust chamber igniter of the VULCAIN HM60 liquid propellant rocket engine for ARIANE 5; other applications are envisaged. Small amounts of selected additives play an important role in solving some of the problems presented by propellants that include ammonium nitrate (AN). The phase transition IV → III which occurs at 305 K (32 °C) and the associated large volume change of the AN crystal is a serious problem. Incorporation of small amounts of NiO (1–3 wt%) in the AN crystal lattices produces one kind of phase-stabilised ammonium nitrate (PSAN) by promoting the AN phase transition from IV to II, which eliminates the previously mentioned abrupt volume change in the useful temperature range [1, 2]. Other problems presented by AN propellants are their high hygroscopicity, low ignitability and low burning rate. Korting et al. [3] found that in the range 1.5–10 MPa, Fe_2O_3 improves the ignitability of AN/HTPB propellants and when used in small quantities (0.4–0.5 wt%), it increases the pre-exponential factor moderately and the pressure exponent slightly of Vieille's burning-rate law; when Fe_2O_3 was increased (1.0–4.0 wt%), a decrease in the pre-exponential factor and pressure exponent was observed. (Vieille's law is an empirical, dimensional non-homogeneous law, named after the French combustion engineer and scientist Paul Vieille (1854–1934), and used to describe the dependence of steady-state burning rate of solid propellants on pressure, at a fixed initial temperature of the propellant and under zero cross-flow; it has the form $r = ap^n$, where r is the burning rate in mm s^{-1}, a the pre-exponential factor, p the burning pressure in MPa, and n the pressure exponent.) Korting et al. [3] also found

that when Fe_2O_3 is used in very small amounts (0.25 wt%) it may cause combustion instability. Langlet et al. [4] found, using mass spectrometry, that in the combustion of ammonium perchlorate (AP) AP/HTPB propellants, Fe_2O_3 has an effect not only on AP decomposition but also on HTPB decomposition. Carvalheira [5] used TGA and found no effect of Fe_2O_3 on AN slow thermal decomposition confirming the observation of Guiochon [6]. These observations and results of Langlet et al. [4] indicate that the effect of Fe_2O_3 on burning rate of PSAN/HTPB propellants as shown by Korting et al. [3] must be in the decomposition of HTPB, even if a gas-phase catalytic mechanism involving this iron compound is not out of question. Fe_2O_3 is a very convenient burning-rate catalyst because it has a considerable effect even if used in small quantities, it introduces no appreciable changes in the Vieille's law pressure exponent, it is cheap and easily available, it presents no compatibility problems with other propellant ingredients and if particle size and shape are conveniently chosen it introduces no undesirable effects on rheological properties during propellant manufacture [7]. Although the effect of Fe_2O_3 as a burning-rate modifier in PSAN/HTPB propellants is well known, its mechanism of action is not well understood. The main objective of this work is to investigate the mechanism of action of Fe_2O_3 as a burning-rate modifier on PSAN/HTPB propellants using thermogravimetry (TG), differential thermogravimetry (DTG) and differential thermal analysis (DTA). TG, DTG and DTA have been applied to study the slow thermal decomposition of selected compositions including, as ingredients, PSAN (called the oxidizer in composite solid rocket-propellant nomenclature), HTPB cross-linked with isophorone diisocyanate (IPDI) (the binder system, called the binder in abbreviated form), and Fe_2O_3 (the burning-rate catalyst), of a PSAN/HTPB–IPDI/Fe_2O_3 composite solid-propellant system. It was found that Fe_2O_3 changes the kinetics of the first stage of HTPB–IPDI decomposition and increases the exothermicity of the HTPB–IPDI decomposition. The effect of Fe_2O_3 is also observed at the beginning of the second stage of decomposition of PSAN/HTPB–IPDI/Fe_2O_3 propellants which is the first stage of decomposition of HTPB–IPDI in these compositions. This is a very important result because for polybutadiene (PB), as the heating rate increases the weight loss by the mechanism of the first step of decomposition of polybutadiene becomes dominant [8,9], and high heating rates are characteristic of combustion-like conditions. A synergetic exothermic interaction between PSAN and HTPB–IPDI is found in PSAN/HTPB–IPDI/Fe_2O_3 propellants. A physical-chemical explanation is given for this interaction based on the fact that AN decomposition becomes less endothermic and even exothermic as pressure increases [10] and on thermal oxidation of the binder by the products of decomposition and dissociation of PSAN. It was found that Fe_2O_3 has no effect on PSAN decomposition, as previous workers [5,6] found for AN decomposition.

2. Experimental

2.1. Materials

PSAN containing 1 wt% NiO, as phase-stabilising agent, and 0.5 wt% Petro, as anti-caking agent, with a particle size diameter d_p of 180 μm, was obtained from ICT, Germany. The particle size of PSAN was measured using a Malvern particle sizer 2600

with a powder-in-air method at 15% RH and 20°C ambient temperature. HTPB Poly Bd R45HT was obtained from Atochem. According to the manufacturer's information for this HTPB, the molecular weight is 2800 g Eq^{-1}, the hydroxyl value is 0.83 meq g^{-1}, the hydroxyl number is 46.6 mg KOH g^{-1}, *trans*-1,4 content is 60%, *cis*-1,4 content is 20%, and vinyl-1,2 content is 20%. The hydroxyl number was measured and found to be 46.5 mg KOH g^{-1}. IPDI was obtained from Fluka Ref. 59192, and Fe_2O_3 BayFerrox 180 (purity, 96–97% , $d_p = 0.7$ μm) was obtained from Bayer Chemie A.G.

2.2. Sample preparation

Samples were prepared in a climate-controlled room with 15–20% RH and 18–23°C ambient temperature. Samples of PSAN were collected from the PSAN container. The same was valid for the HTPB sample. PSAN/Fe_2O_3 samples were prepared by careful mechanical mixing of the two components in a 5 cm diameter polished-porcelain container with a polished-porcelain pylon. PSAN/HTPB–IPDI/Fe_2O_3 samples were prepared in a polyethylene container by first mixing manually HTPB and Fe_2O_3 (if present in the composition), for 20 min, then adding PSAN (if present in the composition), and mixing again manually for 10 min, and finally adding IPDI and mxing for 30 min. Compositions containing HTPB and IPDI were allowed to cure in an oven at 303 K (60°C), for 10 days at atmospheric pressure. Isophorone diisocyanate (IPDI) is the curing agent for HTPB. A ratio of NCO:OH = 0.90 was used for all compositions.

2.3. Apparatus and procedure

TG/DTA measurements were carried out using a Seiko TG/DTA 320. Prior to the experiments, calibration was performed using melting points of pure indium (Fluka, purity: 99.999%) and tin (from Seiko sample kit of standards, purity > 99.99%). For all samples, a mass of 10–11 mg was used, and a heating rate of 10 K min^{-1}. The purging gas was N_2 (dry), at a 40 ml min^{-1} gas flow rate and at 0.1 MPa absolute pressure. Care was taken to avoid contact with moisture during storage before the measurements and during measurements, because of the high hygroscopicity of PSAN. Before the measurements, samples were stored in a room at a relative humidity of less than 20% and a temperature of 18–23°C, and measurements were made in a room within the same ambient conditions. Transportation of the samples from the preparation laboratory to the thermal analysis laboratory was made in sealed polyethylene bags containing dried silica gel. For compositions 1, 2, 3 and 4, the initial and final temperatures were respectively 298 K (25°C) and 648 K (375°C). Table 1 gives the compositions tested. For the other samples, the initial and final temperature were respectively 303 K (30°C) and 848 K (575°C). Two measurements were taken for each composition.

2.4. Methodology of analysis

2.4.1. TG/DTA measurements

The DTA signals are indicated in Kelvin and the temperature sensor is a Pt–Pt13%Rh thermocouple measuring temperature difference between the sample in an

Table 1
Sample composition and size

Composition	PSAN/wt%	HTPB/wt%	IPDI/wt%	Fe_2O_3/wt%	Sample size/mg
1	100	0	0	0	10
2	99.500	0	0	0.500	10
3	99.000	0	0	1.000	11
4	97.500	0	0	2.500	10–11
5	0	100	0	0	10–11
6	0	92.334	7.666	0	10–11
7	0	91.411	7.589	1.000	10–11
8	0	90.026	7.474	2.500	10
9	75.000	23.084	1.916	0	11
10	74.625	23.084	1.916	0.375	10
11	74.250	23.084	1.916	0.750	10–11
12	73.125	23.084	1.916	1.875	10

open aluminium pan and an empty aluminium pan as reference. The amplitude of the DTA peaks ΔT and the temperature of the sample at maximum amplitude of the DTA peaks T_m were considered, rather than the onset temperatures of the DTA peaks T_0, because they are unambiguously defined. Results of DTA measurements expressed as DTA peak amplitudes and temperature of samples are presented in Table 2. The temperature, magnitude and weight loss fraction of DTG peaks for the decomposition stages are presented in Table 3.

2.4.2. Kinetics of decomposition at 10 K min^{-1}

Kinetic parameters such as activation energies and pre-exponential factors were calculated using the non-isothermal method developed by Coats and Redfern [11] to analyse the TG data. This method is subject to some criticism and has been compared by Sharp and Wentworth [12, 13] with the method developed by Freeman and Carroll [14] and with the method developed by Achar et al. [15] to study the kinetics of decomposition of calcium carbonate, both pure and with some additives, as a loose powder and in pellet form. It proved to give satisfactory results and to be less time-consuming than the other methods. This makes it convenient for use when a large number of experiments is needed to characterise a material or a combination of materials when compared to the isothermal methods. Recently, it has been used by Chen and Brill [16, 17] to determine the kinetic parameters of decomposition and thermolysis at low heating rates (1–10 K min^{-1}) of polymeric binders used in composite solid propellants. Arrhenius kinetic parameters obtained using isothermal TGA and this method were found to be essentially the same for both methods within experimental errors for energetic azide polymeric binders [16].

The equations used are presented below

$$\frac{dT}{dt} = \beta \tag{1}$$

Table 2
DTA peak amplitude (K) and temperature (K) of samples

Composition	1st		2nd		3rd		4th		5th		6th	
	T_m	ΔT	T_m	ΔT	T_m	ΔT	T_m	ΔT	T_m	ΔT	T_m	ΔT
1	337	−0.66	412	−1.4	452	−1.3	568	−4.9				
2	336	−0.67	407	−1.4	448	−1.3	567	−4.8				
3	337	−0.66	407	−1.4	448	−1.2	566	−4.7				
4	337	−0.66	409	−1.4	450	−1.2	564	−4.8				
5	649	+1.9	725	−0.41	752	−0.67						
6	638	+0.80	717	−0.34	747	−0.46						
7	636	+0.91	724	−0.41	742	−0.35						
8	636	+1.02	723	−0.46	741	−0.3						
9	339	−0.7	406	−1.2	443	−1.1	501	+4.7	526	−2.3		
10	339	−0.6	406	−1.2	443	−1.2	505	+4.2	527	−1.4		
11	338	−0.6	405	−1.2	443	−1.2	505	+4.2	529	−1.3	754	−0.3
12	338	−0.6	406	−1.2	444	−1.2	506	+5.9	526	−0.8		

Table 3
Temperature, magnitude and weight loss fraction of DTG peaks in decomposition stages

Comp.	1st peak			2nd peak			3rd peak			Residue/wt%
	T_m/K	Deriv. weight/(% K^{-1})	Weight loss/wt%	T_m/K	Deriv. weight/(% K^{-1})	Weight loss/wt%	T_m/K	Deriv. weight/(% K^{-1})	Weight loss/wt%	
	1st stage									
1	565	2.54	99.1							0.9
2	564	2.57	99.1							0.9
3	563	2.52	98.8							1.2
4	560	2.59	97.8							2.2
	1st stage			2nd stage						
5	660	0.205	10.8	723	2.21	34.1	738	1.97	55.1	0
6	637	0.218	14.8	723	1.60	38.6	740	1.76	45.9	0.7
7	630	0.173	12.1	721	2.39	35.9	739	2.12	50.4	1.6
8	629	0.188	12.6	722	2.40	36.4	742	1.99	48.2	2.8
	1st stage						2nd stage			
9	502	14.15	49.1	515	1.01	24.8	719	0.397	19.2	6.9
10	505	14.4	50.2	520	1.13	23.8	718	0.396	19.3	6.7
11	504	12.2	47.6	520	1.32	25.1	718	0.412	18.7	8.6
12	505	13.7	50.7	518	1.11	21.1	717	0.387	19.0	9.2

$$\alpha = \frac{m_0 - m}{m_0} \tag{2}$$

$$\frac{d\alpha}{dt} = k(T)(1-\alpha)^n \tag{3}$$

According to Guiochon [6], AN thermal decomposition is first order. Chen and Brill [17] have considered the thermal decomposition of HTPB prepolymer and cross-linked HTPB–IPDI polymer to be first order. Assuming a first-order decomposition for all compositions, as a first approximation, we have $n = 1$ [11]

$$k(T) = A \exp\left(-\frac{E}{RT}\right) \tag{4}$$

$$\ln\left(\frac{-\ln(1-\alpha)}{T^2}\right) = \ln\left[\frac{AR}{\beta E}\left(1 - 2\left(\frac{RT}{E}\right)\right)\right] - \frac{E}{RT} \tag{5}$$

The criterion we have used to select the data range to determine the kinetic parameters was the large-range linearity criterion where we chose the largest data range where there is a linear dependence of $\ln(-(\ln(1-\alpha))/T^2)$ on $1/T$. The criterion for linearity to select the largest $(1-\alpha)$ range was visual observation of the graphs, at first, and then, in a more accurate way, imposing the correlation coefficient of the linear regression of the data to be larger than 0.99. The Arrhenius kinetics parameters in Table 4 are the results of application of the large-range linearity criterion to the TG data.

For compositions 9, 10, 11 and 12 (see Table 1), a slightly different algorithm was used to calculate kinetic parameters by the non-isothermal TG method, for two

Table 4
Arrhenius parameters obtained by the non-isothermal TG method with large-range linearity criterion [a]

Comp.	1st stage			2nd stage		
	$\log A/s^{-1}$	E/(kJ mol^{-1})	$(1-\alpha)$ range	$\log A/s^{-1}$	E/(kJ mol^{-1})	$(1-\alpha)$ range
1	8.53±0.03	113.5±0.5	0.87–0.53			
2	8.63±0.10	114.2±0.9	0.85–0.47			
3	8.64±0.16	114.2±1.5	0.85–0.48			
4	8.63±0.13	114.0±1.2	0.86–0.46			
5	2.59±0.10	77.0±1.4	0.98–0.82	13.20±0.21	215.4±2.9	0.62–0.045
6	1.41±0.26	59.5±2.8	0.98–0.76	11.59±0.49	192.5±6.7	0.60–0.030
7 [b]	1.45	61.4	0.99–0.77	11.52	206.1	0.53–0.049
8	2.17±0.36	69.4±4.7	0.99–0.76	11.78±0.43	196.1±5.9	0.55–0.069
9	9.99±1.10	118.5±10.4	0.98–0.79 [c]	20.2±3.9	311±54	0.91–0.70 [d]
10	9.37±0.64	112.0±6.5	0.96–0.69 [c]	21.6±1.8	329±25	0.97–0.76 [d]
11	8.84±1.47	108.4±13.6	0.97–0.73 [c]	31.1±8.9	458±119	0.96–0.81 [d]
12	10.19±0.63	120.4±6.3	0.97–0.70 [c]	35.8±7.5	524±102	0.97–0.87 [d]

[a] Errors are based on the standard deviation of the actual points and the least square fit.
[b] Only one measurement made for this composition.
[c] $(1-\alpha)^*$ range.
[d] $(1-\alpha)^{**}$ range.

reasons. Firstly, observation of the TG curves suggests the existence of two stages at two different temperature ranges corresponding to the decomposition of the two main constituents of these compositions, namely PSAN and cross-linked HTPB–IPDI; secondly, a correlation was envisaged with the temperature ranges and slow decomposition kinetic parameters of the main constituents of these propellant compositions, namely PSAN and cross-linked HTPB–IPDI, with and without Fe_2O_3.

Basically the algorithm and equations are the same as the previous ones, but are applied to two different stages. The first stage corresponds to a condition where the mass fraction decomposition is less or equal to the oxidiser and additives mass fraction; the second stage corresponds to the decomposition of the remainder of the sample. For the first and second stages, $(1-\alpha)$ is substituted respectively by $(1-\alpha)^*$ and $(1-\alpha)^{**}$ in all equations where it appears

$$(1-\alpha)^* = \frac{m - m_0 f_b}{m_0(1-f_b)} \quad \text{for } 1.00 > (1-\alpha) > f_b \tag{6}$$

$$(1-\alpha)^{**} = \frac{m}{m_0 f_b} \quad \text{for } f_b > (1-\alpha) > 0 \tag{7}$$

3. Results and discussion

3.1. PSAN/Fe_2O_3 compositions

The TG/DTA and DTG curves of PSAN powder without Fe_2O_3 are shown in Fig. 1. TG and DTA curves of PSAN powder coated with different concentrations of Fe_2O_3 are similar to the respective TG and DTA curves of PSAN powder shown in Fig. 1. For

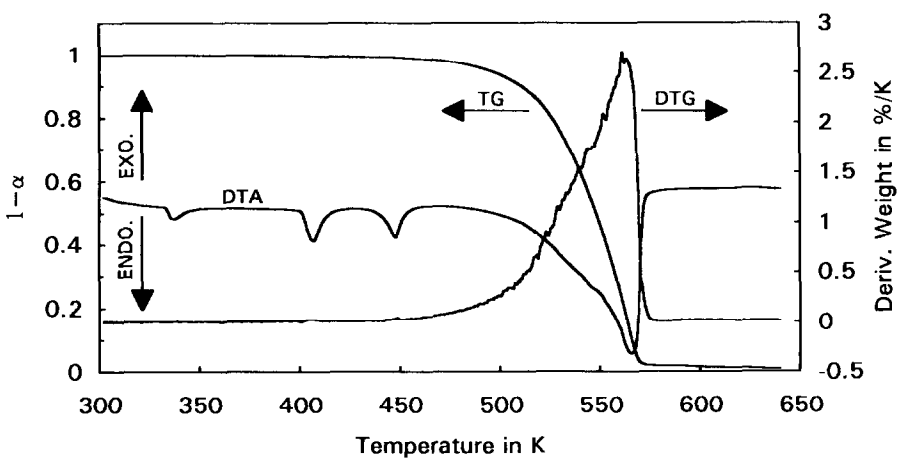

Fig. 1. TG, DTG and DTA results for PSAN powder without iron(III) oxide. In all figures, data are obtained at a heating rate of 10 K min^{-1}, under a 40 ml min^{-1} nitrogen flow.

TG and DTG curves, there is a small difference between PSAN powder and PSAN powder coated with different concentrations of Fe_2O_3. For DTA curves the addition of Fe_2O_3 to PSAN causes a reduction in T_m of less than 5 K in the phase transition II → I, on melting and on the last endothermic peak. Observation of the plots of $\ln(-(\ln(1-\alpha))/T^2)$ vs. $1/T$ suggests only one step need be considered for decomposition of samples of these compositions. Kinetic parameters obtained by the non-isothermal method for these compositions are presented in Table 4. They indicate almost no effect of Fe_2O_3 on either log A or E when it is added to PSAN, and there is no net trend, within experimental uncertainty, in the evolution of the values of either of these kinetic parameters with increasing Fe_2O_3 mass fraction. This indicates no effect of Fe_2O_3 on PSAN decomposition kinetic parameters, and a small effect on the phase transition from II to I and on melting of PSAN, shown by the DTA peaks.

3.2. *HTPB IPDI/Fe_2O_3 compositions*

HTPB is composed of a mixture of *trans*-1,4-, *cis*-1,4- and vinyl 1,2-polybutadiene isomers. The relative amount of the isomers can be controlled in the synthesis process but all three exist in propellant-grade HTPB. The TG/DTA and DTG curves of HTPB prepolymer are shown in Fig. 2 where two main DTG peaks can be seen. In the second main peak, two secondary peaks can be considered, as also reported by Tingfa Du [18]. Table 3 shows the DTG data relative to these peaks. In addition, observation of DTA and DTG curves in Fig. 2 shows that the first DTG peak weight loss is an exothermic stage and that the two other DTG peaks weight losses are endothermic. The overall pattern of the TG, DTA and DTG curves is in agreement, respectively, with the TG, DSC, and DTG results reported by previous workers for HTPB [17, 18] and PB [8, 9] with the same heating rate and 4–6 mg samples. The weight loss in the first stage of decomposition of HTPB is mainly due to depolymerisation of HTPB where lower

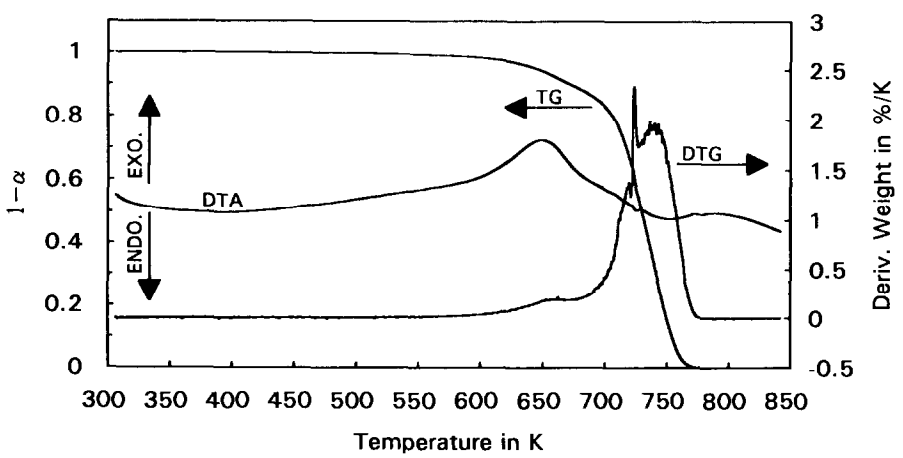

Fig. 2. TG, DTG and DTA results for HTPB prepolymer.

molecular weight hydrocarbons, such as 1,3-butadiene (C_4H_6) and 4-vinylcyclohexene (C_8H_{12}), volatilise [17]. In the first stage, cyclisation and cross-linking of the HTPB occur simultaneously. Depolymerisation is an endothermic process, while cross-linking and cyclisation are exothermic processes. Material not undergoing depolymerisation cyclises and cross-links, yielding a solid residue which decomposes in the second stage [17]. The first stage is an overall exothermic process as a result of the positive energy balance of the endothermic depolymerisation process and the exothermic cross-linking and cyclisation [17]. The second stage of decomposition of HTPB is endothermic because of the predominance of bond-breaking (depolymerisation) of the cross-linked residue from the first stage and desorption of the fragments [17]. These processes are essentially the same as those that occur with PB [8, 9, 19]. For PB, in the first stage, the competition between depolymerisation and cross-linking and cyclisation is evidenced by the facts that when heating rate is increased the weight loss in the first stage increases, and the amount of 1,3-butadiene in the volatile products increases while the amount of 4-vinylcyclohexene is maintained. In the first stage at $\beta = 10\,K\,min^{-1}$, weight loss is 5–11 wt% for HTPB [this work, 18] and for PB [9], while at $\beta = 100\,K\,min^{-1}$ it is about 50 wt% for PB [9]. In consequence, it is expected that in combustion-like conditions the first stage of decomposition will dominate the thermal degradation of HTPB, while cross-linking and cyclisation will be negligible. This reasoning is supported by results on the thermal decomposition of HTPB in combustion-like conditions [17] where the kinetic parameters of the process at high heating rate are much closer to the kinetic parameters of the first stage than to those of the second stage of decomposition and where the several diisocyanate cross-linking agents have an effect on the kinetics of thermal decomposition of cross-linked HTPB at high heating rate and on the kinetics of the first stage of decomposition at low heating rate, but not on the thermal decomposition kinetics of the second stage of decomposition. In consequence of this, for our purposes of evaluating the effect of iron(III) oxide on the thermal decomposition of HTPB in combustion-like conditions, using slow thermal decomposition, the effect of this additive in the first stage of decomposition assumes primary relevance.

TG/DTA and DTG curves of cross-linked HTPB–IPDI polymer have a pattern similar to those of HTPB prepolymer in Fig. 2. Compared to the TG/DTA and DTG curves of HTPB prepolymer, the most important differences are: the reduction from 649 to 638 K and the reduction in amplitude from 1.9 to 0.8 K of the first DTA exothermic peak; the reduction in magnitude, from -0.41 to -0.34 K, and in T_m, from 725 to 717 K, for the second DTA peak; the reduction in magnitude, from -0.67 to -0.46 K, and in T_m, from 752 to 747 K, for the last main endothermic peak; the reduction from 660 to 637 K of the first DTG peak; an increase in the weight loss fraction of the first and second steps of decomposition, in consequence of higher IPDI volatility; and a decrease in the weight loss of the third DTG peak. For the DTG curve, we also obtained a main DTG peak which, in our DTG curve, includes two secondary DTG peaks. Chen and Brill [17] used the same method to study the slow decomposition of pure HTPB and cross-linked HTPB–IPDI with a NCO:OH ratio of 1.0 and with samples about half the mass (4–6 mg) of ours (10–11 mg). For cross-linked HTPB–IPDI with 10 K min^{-1} heating rate, Chen and Brill [17] obtained just one

endothermic DTG peak. The first weight loss stage is probably associated with depolymerisation and cleavage of urethane cross-links. In this first stage there is also cross-linking and cyclisation of the HTPB backbone which do not contribute to any noticeable weight loss but are responsible for the overall exothermic character of the first stage of the decomposition. The two other weight losses are depolymerisation of the cross-linked and cyclised residue from the first stage of decomposition and are overall endothermic processes [17]. As shown in Table 5, the value of E obtained in our measurements is in agreement, within experimental error, with the value obtained by Chen and Brill [17] for pure HTPB for the first stage and for cross-linked HTPB–IPDI for the second stage of decomposition. The value of E for the second stage and the values of log A for the first and second stages for pure HTPB, and for the second stage of cross-linked HTPB–IPDI decomposition obtained in this work are close to the values obtained by Chen and Brill [17] but are not in agreement with their results within experimental error.

DTA curves for HTPB prepolymer, cross-linked HTPB–IPDI polymer and HTPB–IPDI/Fe_2O_3 polymer with different concentrations of Fe_2O_3 are shown in Fig. 3, and DTA peak data are shown in Table 2. When Fe_2O_3 is added to cross-linked HTPB–IPDI the following trends are shown with increasing Fe_2O_3 content: the first exothermic peak shows a slight increase in magnitude and almost no change in T_m and a net increase in area; the first endothermic peak shows an increase in magnitude, becoming higher than the second endothermic peak, and an increase in T_m; the second endothermic peak shows a reduction in magnitude and T_m; the magnitude of the area of the endothermic peaks is reduced and that of the exothermic peaks is increased; the overall decomposition process becomes more exothermic.

DTG curves of HTPB prepolymer, cross-linked HTPB–IPDI and HTPB–IPDI/Fe_2O_3 polymer with different concentrations of Fe_2O_3 are similar in shape. Table 3 shows the DTG peaks, weight loss and residue data. When Fe_2O_3 is added to cross-linked HTPB–IPDI, there is a decrease in magnitude and weight loss fraction, and a 7–8 K reduction in T_m for the first peak; there is an increase in magnitude, a decrease in the weight loss fraction and a 1–2 K decrease in T_m for the second and largest peak; and an increase in magnitude and weight loss fraction and almost no

Table 5
Comparison of Arrhenius parameters obtained by the non-isothermal TG method in this work and in other investigations

Ref.	Composition	1st stage			2nd stage		
		log A/s^{-1}	E/(kJ mol^{-1})	T/K	log A/s^{-1}	E/(kJ mol^{-1})	T/K
This work	HTPB	2.59±0.10	77.0±1.4	608–703	13.20±0.21	215.4±2.9	722–759
	HTPB–IPDI	1.41±0.26	59.5±2.8	572–695	11.59±0.49	192.5±6.7	717–760
[17][a,b]	HTPB	1.1	78.7	601–693	10.1	195	709–743
	HTPB–IPDI				9.8	192	709–743

[a] Values of E converted from kcal mol^{-1} in Ref. [12] to kJ mol^{-1} by multiplying by 4.184.
[b] Values of T converted from °C in Ref. [12] to K by adding 273.15.

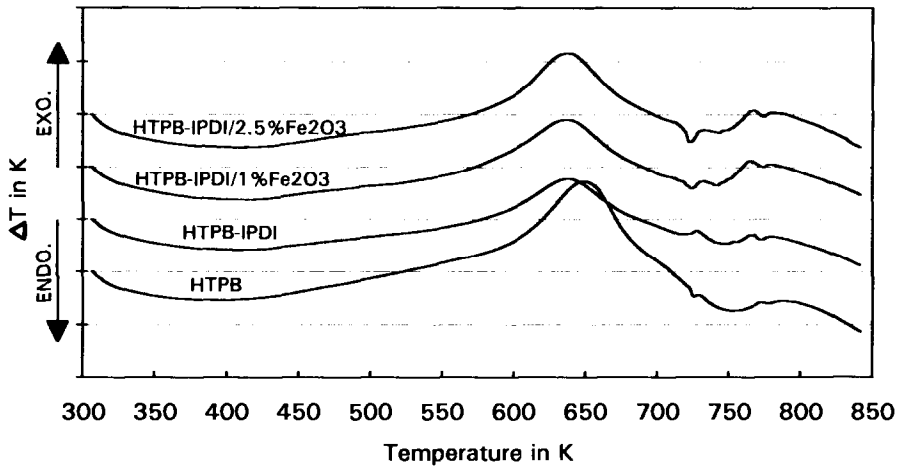

Fig. 3. DTA results for HTPB prepolymer, cross-linked polymers HTPB–IPDI and HTPB–IPDI/Fe_2O_3 with different concentrations of Fe_2O_3.

change in temperature for the third and also large peak. The weight loss fraction distribution of cross-linked HTPB–IPDI/Fe_2O_3 lies between that of HTPB and that of cross-linked HTPB–IPDI. The residue increases from HTPB to cross-linked HTPB–IPDI and when Fe_2O_3 is added continues to increase, but this increase can be mainly accounted for by added Fe_2O_3.

The net increase in the amplitude of the first DTA exothermic peak with increasing Fe_2O_3 mass fraction, the reduced mass loss and mass loss rate of the correspondent first DTG peak with inclusion of Fe_2O_3 indicate that Fe_2O_3 promotes cross-linking and cyclisation (exothermic processes) and reduces depolymerisation in the first stage of decomposition of cross-linked HTPB–IPDI and there is a pattern of higher regression rates with higher rigidity in linear pyrolysis studies with other polymers [20].

As suggested by observation of $\ln(-(\ln(1-\alpha))/T^2)$ vs. $1/T$ plots and previous work by Chen and Brill [17], two steps were considered for the decomposition of samples of compositions 5, 6, 7 and 8. Arrhenius plots for the kinetics of weight loss measured by TG for HTPB, cross-linked HTPB–IPDI polymer and HTPB–IPDI/Fe_2O_3 propellants with different concentrations of Fe_2O_3 are shown in Fig. 4. Arrhenius parameters obtained by the non-isothermal method for compositions 5, 6, 7 and 8 are presented in Table 4. When Fe_2O_3 is added to cross-linked HTPB–IPDI (compositions 6, 7 and 8) and Fe_2O_3 mass fraction is increased, there is a monotone increase in both log A and E for the first stage of decomposition and, in general, the kinetics of decomposition of cross-linked HTPB–IPDI/Fe_2O_3 approaches the TG kinetics of decomposition of pure HTPB, indicating a net effect of Fe_2O_3 on the first stage of decomposition of cross-linked HTPB–IPDI. The second stage of decomposition is very similar for compositions 6, 7 and 8. They indicate that for both log A and E there is a noticeable reduction in first stage and second stage of decomposition from pure HTPB to cross-linked HTPB–IPDI. For the second stage, there is no definite trend in the

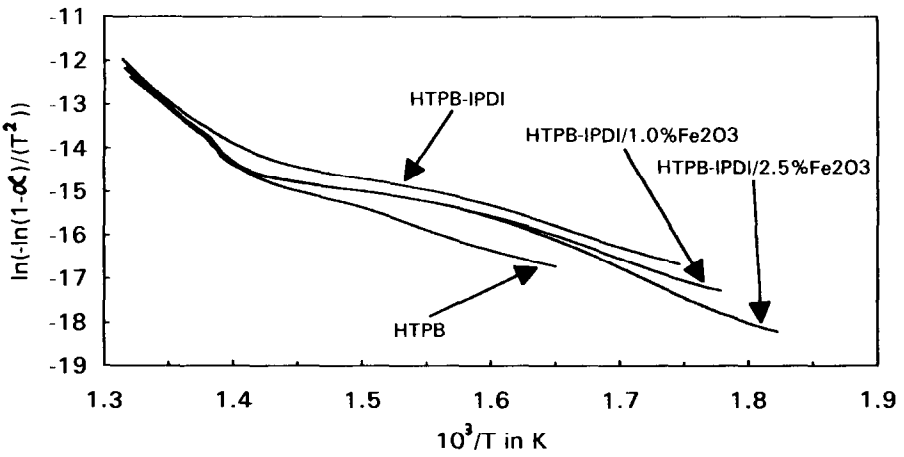

Fig. 4. Arrhenius plots for the kinetics of weight loss measured by TG for HTPB prepolymer, cross-linked polymers HTPB IPDI and HTPB–IPDI/Fe_2O_3 with different concentrations of Fe_2O_3. The second stage of decomposition is very similar for cross-linked polymers HTPB–IPDI and HTPB–IPDI/Fe_2O_3 with different concentrations of Fe_2O_3.

evolution of either log A or E with increasing Fe_2O_3 content and the values overlap or almost overlap within experimental error. In the first and second stages, results for the Arrhenius kinetic parameters of compositions 5, 6, 7 and 8 show relatively low dispersion.

3.3. *PSAN/HTPB-IPDI/Fe_2O_3 compositions*

Fig. 5 illustrates typical TG, DTG and DTA curves of PSAN/HTPB–IPDI propellant. TG, DTG and DTA curves of PSAN/HTPB–IPDI/Fe_2O_3 compositions are similar in shape to TG, DTG and DTA curves of PSAN/HTPB–IPDI. The three first endothermic peaks, corresponding respectively to the phase transitions IV → II, II → I and to melting of PSAN [2], show T_m values close to the values for PSAN. For the PSAN/HTPB–IPDI composition, a strong DTA exothermic peak appears at 501 K and a strong DTG peak appears at 502 K. This is the strongest effect observed for all compositions and is a synergetic solid phase reaction that is present in propellant samples containing PSAN and cross-linked HTPB–IPDI. This synergetic effect is also present at 504–506 K in PSAN/HTPB–IPDI/Fe_2O_3 compositions. The exothermic peaks of DTA curves are the most intense and the intensity of this first DTG peak oscillates in the range 12.2–14.4 wt% K^{-1} for these compositions. For PSAN/HTPB–IPDI and PSAN/HTPB–IPDI/Fe_2O_3 compositions, there is also an endothermic peak that is not present for the other compositions. This peak is in the temperature range 526–529 K and becomes less endothermic with increasing Fe_2O_3 content. A related DTG peak was observed at 515 K for PSAN/HTPB–IPDI and in the range 518–520 K for PSAN/HTPB–IPDI/Fe_2O_3 compositions with no monotone change in magnitude with increase in Fe_2O_3 content. There are also DTG peaks at 719 K for

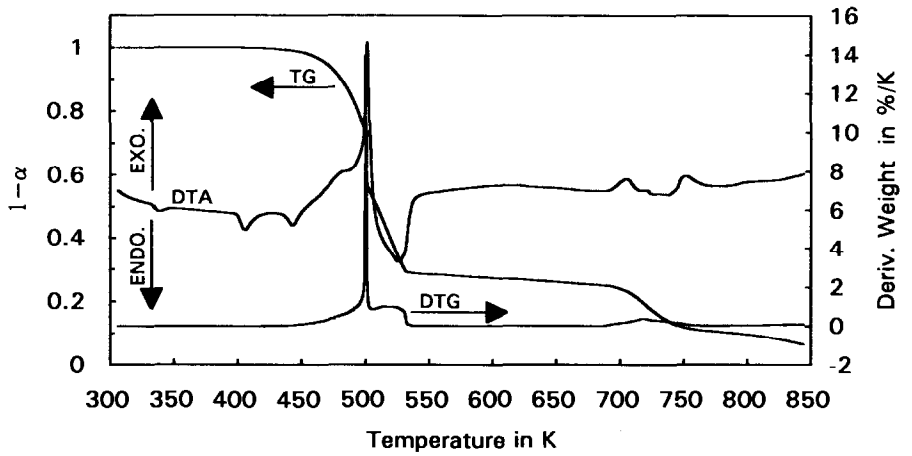

Fig. 5. TG, DTG and DTA results for PSAN/HTPB–IPDI propellant.

PSAN/HTPB–IPDI and at 717–718 K for PSAN/HTPB–IPDI/Fe_2O_3 compositions with no appreciable change in magnitude with increase in Fe_2O_3 content. The endothermic DTA peak at 754 K for PSAN/HTPB–IPDI/Fe_2O_3 containing 0.75 wt% Fe_2O_3 is related to the decomposition of the HTPB–IPDI weight fraction in compositions PSAN/HTPB–IPDI/Fe_2O_3 because it appears, respectively, as an endothermic DTA peak in the second stage of decomposition of HTPB–IPDI at 747 K and in the second stage of decomposition of HTPB–IPDI/Fe_2O_3 compositions at 741–742 K. The two exothermic DTA peaks respectively at about 700 and 750 K shown in Fig. 5 are particular to one of the two measurements made with PSAN/HTPB–IPDI composition and are not repeatable patterns.

Observation of the $\ln(-(\ln(1-\alpha))/T^2)$ vs. $1/T$ plot of composition 9, in Fig. 6, suggests four steps of decomposition. Plots of $\ln(-(\ln(1-\alpha))/T^2)$ vs. $1/T$ for compositions 10, 11 and 12 present the same pattern as composition 9. The first step was identified as PSAN decomposition. The second step is considered a runaway in weight loss of PSAN for which a physical explanation is given later. The third step is a relaxation of the previous runaway process. The fourth step is considered to be the thermal decomposition of the HTPB–IPDI binder mass fraction. We consider the second and third steps to be unrepresentative of the kinetics of thermal decomposition of these propellants at 0.1 MPa and consequently the Arrhenius kinetics parameters were determined only for the first and fourth steps, which were called the first and second stage, respectively.

Table 4 presents TG kinetic parameters for samples of compositions 9, 10, 11, and 12. Analysis of results for first stage indicate that there is no net tendency, within experimental uncertainty, in the evolution of the values of log A and E with increasing Fe_2O_3 mass fraction. As the first stage of decomposition for these compositions is mainly due to PSAN decomposition, this is in agreement with the results for compositions 1, 2, 3 and 4 containing PSAN and Fe_2O_3 which indicate no catalytic effect of

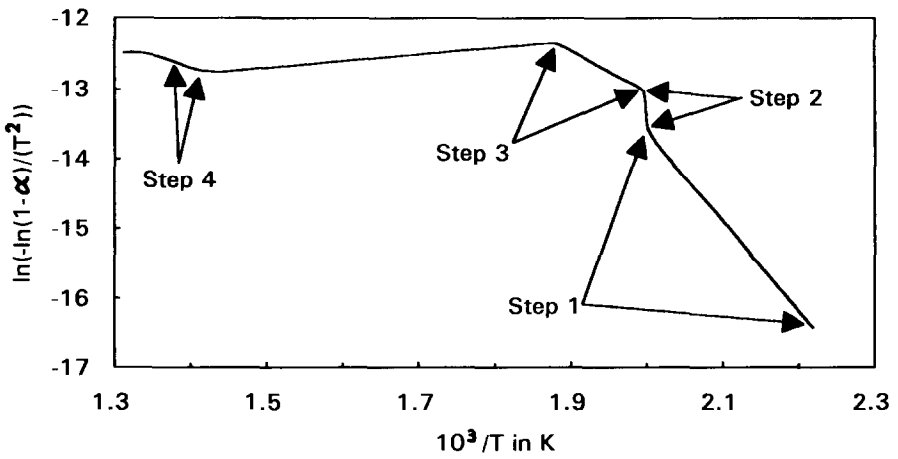

Fig. 6. Arrhenius plots for the kinetics of weight loss measured by TG for decomposition of propellant PSAN/HTPB–IPDI showing four steps in the decomposition process.

Fe_2O_3 on PSAN decomposition. Arrhenius plots for the kinetics of weight loss measured by TG for PSAN/HTPB–IPDI and PSAN/HTPB–IPDI/Fe_2O_3 propellants with different concentrations of Fe_2O_3 for the second stage of decomposition are shown in Fig. 7. For the beginning of the second stage, there is a monotone increase in the values of both E and log A with increasing Fe_2O_3 mass fraction. Because the second stage of decomposition for these compositions is mainly due to cross-linked HTPB–IPDI decomposition and the range of $(1-\alpha)^{**}$ covered is similar to the range of $(1-\alpha)$

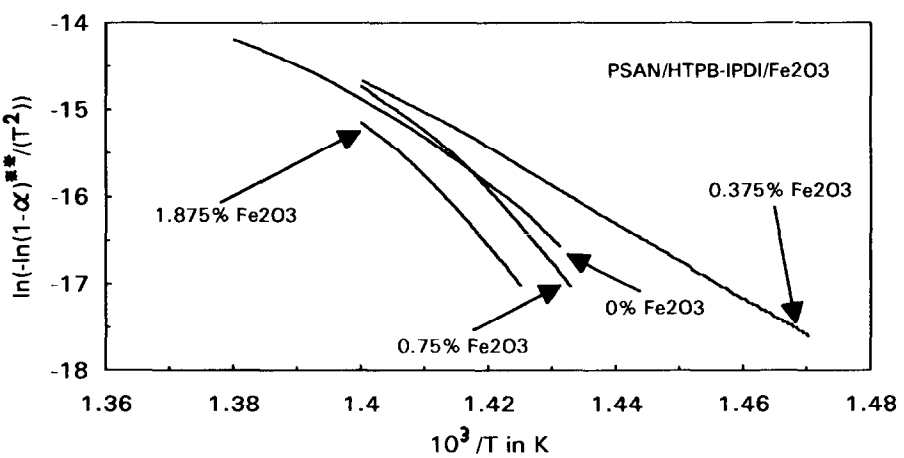

Fig. 7. Arrhenius plots for the kinetics of weight loss measured by TG for the second stage of decomposition of propellants PSAN/HTPB–IPDI and PSAN/HTPB–IDPI/Fe_2O_3 with different concentrations of Fe_2O_3.

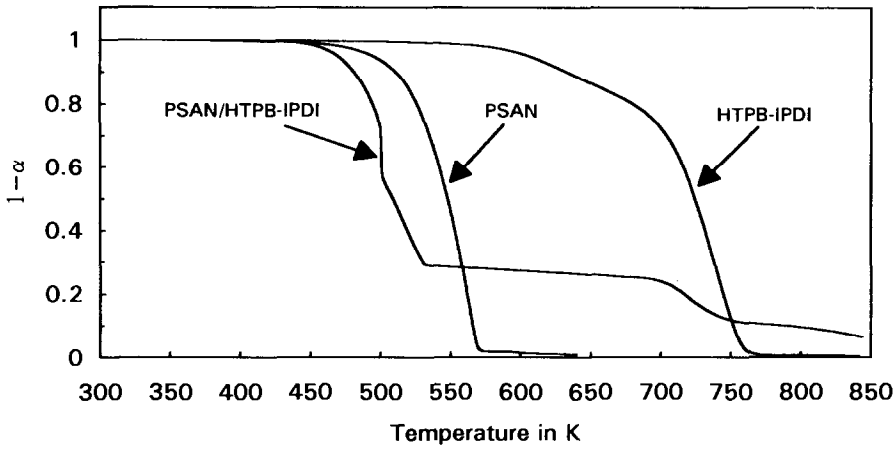

Fig. 8. TG results for PSAN powder, cross-linked HTPB–IPDI polymer and PSAN/HTPB–IPDI propellant.

for first stage of decomposition for compositions 5, 6, 7 and 8 containing cross- linked HTPB–IPDI and Fe_2O_3, this is in agreement with the results for these compositions which indicate a net effect of Fe_2O_3 on the first stage of decomposition of cross-linked HTPB–IPDI decomposition. In the first stage, results for Arrhenius kinetic parameters of compositions 9, 10, 11 and 12 show more dispersion than for compositions 5, 6, 7 and 8, but the results for the second stage show a high level of dispersion especially for compositions 11 and 12.

The interaction between PSAN and HTPB–IPDI in compositions 9, 10, 11 and 12, including PSAN/HTPB–IPDI is evidenced in Fig. 8 by the TG curves of decomposition of bulk PSAN, cross-linked HTPB–IPDI and PSAN/HTPB–IPDI. This interaction is also evidenced by the large DTA and DTG peaks in the 501–506 K range, for the second DTG peak and the corresponding endothermic DTA peak, in Fig. 5, Tables 2 and 3, and for the second and third step in the plot of $\ln(-(\ln(1-\alpha))/T^2)$ vs. $1/T$, shown in Fig. 6, for composition 9 which is representative of compositions 10, 11 and 12 for this interaction. A physical-chemical explanation for this interaction follows. For temperatures higher than the melting point of PSAN (443 K), the decomposition and dissociation process of PSAN begins and oxidising gaseous products begin to be generated. In the propellant, the existence of isolated pockets formed by the binder around each PSAN particle trap these oxidising gaseous products, which begin to oxidise the binder, and produce a pressure inside the pockets that does not occur in the bulk decomposition of PSAN, because in the bulk decomposition of PSAN the gaseous products can escape to the atmosphere through the liquid PSAN–gaseous atmosphere interface. This pressure can make the PSAN decomposition exothermic [10] and may be responsible for the exothermic DTA peak that begins after the melting DTA peak of PSAN in compositions including PSAN/HTPB–IPDI, instead of the endothermic DTA peak that is observed after the bulk melting for PSAN and PSAN/Fe_2O_3

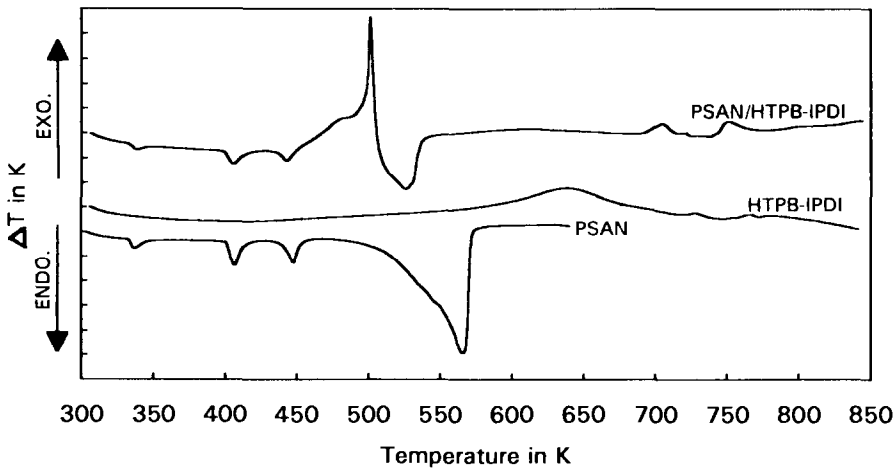

Fig. 9. DTA results for PSAN powder, cross-linked HTPB–IPDI polymer and PSAN/HTPB–IPDI propellant.

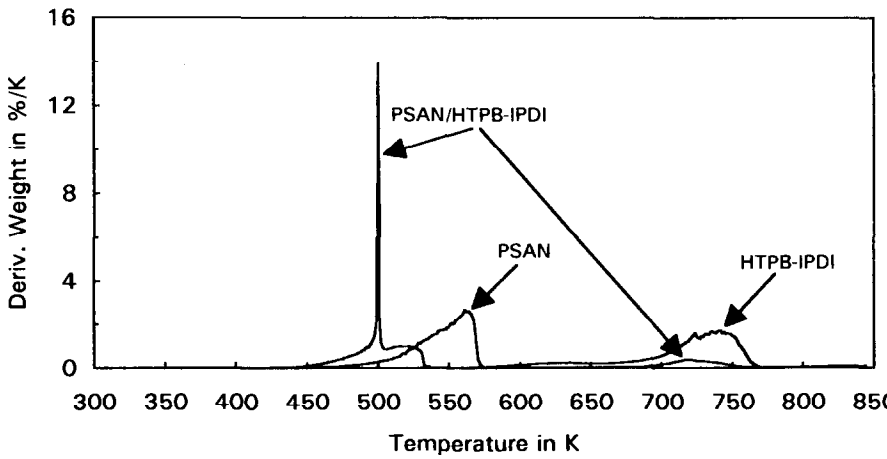

Fig. 10. DTG results for PSAN powder, cross-linked HTPB–IPDI polymer and PSAN/HTPB–IPDI propellant.

compositions, as shown in Fig. 9. Moreover, in the propellant, the specific surface contact area of condensed PSAN with gaseous products of decomposition and dissociation, is larger than in the bulk melted PSAN. Both the pressure build-up and the increase in specific surface contact area of condensed PSAN with these gaseous products increase the decomposition rate. When most of the binder pockets break due to internal pressure build-up they leak the gaseous products and there is a sudden

weight loss of sample which is responsible for the large DTG peak and for the second step in the $\ln(-(\ln(1-\alpha))/T^2)$ vs. $1/T$ plot of Fig. 6. After this, the pressure inside the binder pockets reduces to the ambient pressure of 0.1 MPa and the thermal decomposition of PSAN proceeds. The effect of pressure on PSAN decomposition kinetics and heat generation disappears and consequently the decomposition rate of PSAN decreases strongly as shown by the DTG curves in Fig. 10 for PSAN/HTPB–IPDI composition and bulk PSAN. In addition, the PSAN decomposition becomes endothermic as it is in the last DTA peak of decomposition of bulk PSAN, as shown by the DTA curves in Fig. 9. Only the effect of temperature remains and since these measurements are non-isothermal, as time passes the temperature increase promotes an increase in mass loss rate, attaining a maximum at a certain temperature higher than the temperature of the first exothermic peak. This phase corresponds to the second DTG peak, the corresponding endothermic DTA peak and the third step in the plot of $\ln(-(\ln(1-\alpha))/T^2)$ vs. $1/T$ of Fig. 6. A detail in the shape of the DTG curve of Fig. 5 for PSAN/HTPB–IPDI composition supports this explanation because there is a concordance between the beginning of the envelope of the first DTG peak and the envelope of the second DTG peak. This explanation, being correct, shows the very important role of pressure in the kinetics of PSAN decomposition which can be related to the important effect of pressure on the ignition and combustion of PSAN/HTPB propellants. It would be interesting to estimate the pressure level inside the binder pocket during the first DTG peak and to relate it with the extinction pressure of the propellants of compositions 9–12, which is in the range 1–2 MPa.

A remarkable feature of the TG results for PSAN/HTPB–IPDI and PSAN/HTPB–IPDI/Fe_2O_3 compositions is that they leave an amount of solid residue (6.72–9.16 wt%) that is much higher than the weighted sum, by mass fraction, of the residues of PSAN and HTPB–IPDI compositions plus the weight fraction of Fe_2O_3, which is clearly shown in Fig. 8 for the PSAN/HTPB–IPDI composition. This behaviour can be accounted for by the thermal oxidation at high temperature of HTPB–IPDI polymer by the PSAN oxidiser, because it is well known that in thermal oxidation at high temperature, polymers transform into char leaving more residue than under thermal degradation. The thermal oxidation, at high temperature, of the organic polymer phase HTPB–IPDI by the inorganic oxidiser PSAN could be verified with chemical analysis of the volatiles whose formation would be induced at a lower temperature than in thermal degradation under nitrogen.

The TG/DTG results have less dispersion in peak magnitudes and T_m than the DTA results.

4. Conclusions

There is a strong interaction in the solid phase between PSAN and cross-linked HTPB–IPDI in the propellant composition PSAN/HTPB–IPDI which is revealed by the strong DTA exothermic peak and the strong DTG peak at 502 K. A physical-chemical explanation is given for this interaction. The same strong interaction is observed for the other propellant compositions containing these components and

Fe_2O_3. This additive causes an increase in the magnitude of the exothermic DTA peaks and a decrease in the magnitude of the endothermic DTA peaks.

Compositions including PSAN/HTPB–IPDI (compositions 9–12) exhibit a solid residue which is much greater than the sum of the solid residues weighted by mass fraction of PSAN and HTPB–IPDI plus the solid catalyst mass fraction. This behaviour can be accounted for by the thermal oxidation at high temperature of HTPB–IPDI polymer by the PSAN oxidiser.

When Fe_2O_3 is included as an additive in cross-linked HTPB–IPDI, the overall pattern of DTA curves is maintained for all compositions. The magnitude and shape of the DTA peaks indicate a general increase in exothermicity of cross-linked HTPB–IPDI decomposition with increasing Fe_2O_3 content.

The TG kinetics of decomposition of HTPB, HTPB–IPDI and HTPB–IPDI/Fe_2O_3 compositions, indicate a net effect of Fe_2O_3 in the first stage of cross-linked HTPB–IPDI decomposition. This is confirmed by the TG kinetics results of PSAN/HTPB–IPDI and PSAN/HTPB–IPDI/Fe_2O_3 compositions for the beginning of the second stage of decomposition of these propellants where the first stage of decomposition of HTPB–IPDI occurs.

There is not much difference between the slow thermal decomposition of PSAN and PSAN coated with Fe_2O_3. This is indicated by DTA, TG/DTG and TG kinetics results.

Acknowledgements

We are grateful to Dr. Danny Hoffmans of Prins Maurits Laboratorium and to Dr. Carlos de Sá Furtado of Fundação Calouste Gulbenkian for their encouragement and support. This work was supported by Fundação Calouste Gulbenkian under Grant 5/92/B.

References

[1] R.A.H. Strecker and D. Linde, Gas Generator Propellants for Air-to-Air Missiles, AGARD CP-259, NATO, April 1979.

[2] W. Engel, N. Eisenreich, A. Deimling, M. Hermann, M.J. Lorenzo and V. Kolarik, Ammonium Nitrate, A Less Polluting Oxidizer, 24th Int. Ann. Conf. of ICT 1993, Karlsruhe, Federal Republic of Germany, 1993, p. 3–1.

[3] P.A.O.G. Korting, F.W.M. Zee and J.J. Meulenbrugge, Performance of No Chlorine Containing Composite Propellants with Low Flame Temperatures, AIAA/SAE/ASME/ASEE 23rd Joint Propulsion Conference, June 29–July 2, San Diego, CA, 1987.

[4] A. Langlet, R. Sanden and H. Ostmark, Study of the effect of iron oxide on the degradation of HTPB by mass spectrometry, in Combustion and Reaction Kinetics, 22nd International Annual Conference of ICT 1991, July 2–July 5, Karlsruhe, Federal Republic of Germany, p. 52–1.

[5] P. Carvalheira, Thermal Decomposition of AN. Effect of Chromium(III) and Iron(III) Oxide, Internal Report DEM-FCTUC, 1993, Coimbra, Portugal.

[6] G. Guiochon, La Décomposition Thermique du Nitrate d'Ammonium Pur. Actions Catalytiques de Divers Composés Minéraux, Ann. Chim., 5 (1960) 295–349.

[7] M. Kohno, H. Maruizumi, S. Suzuki, M. Chiba, S. Masuda and K. Kato, Study on Composite Propellants Containing Ferric Oxide, in Proc. 17th Int. Symp. on Space Technology and Science, Tokyo, Vol. I, 1990, p. 227–231.

[8] D.W. Brazier and N.V. Schwartz, The effect of heating rate on the thermal degradation of polybutadiene, J. Appl. Polym. Sci., 22 (1978) 113–124.
[9] K. McCreedy and H. Keskkula, Effect of thermal crosslinking on decomposition of polybutadiene, Polymer, 20 (1979) 1155.
[10] T.P. Russel and T.B. Brill, Thermal decomposition of energetic materials 31—Fast thermolysis of ammonium nitrate, ethylenediammonium dinitrate and hydrazinium nitrate and the relationship to burning rate, Combustion and Flame, 76 (1989) 393–401.
[11] A.W. Coats and J.P. Redfern, Kinetic parameters from thermogravimetric data, Nature, 201 (1964) 68–69.
[12] J.H. Sharp and S.A. Wentworth, Kinetic analysis of thermogravimetric data, Anal. Chem., 41 (1969) 2060–2062.
[13] S.A. Wentworth and J.H. Sharp, Kinetic parameters from thermogravimetric data—a reply, Anal. Chem., 42 (1970) 1297.
[14] E.S. Freeman and B. Carroll, J. Phys. Chem., 62 (1958) 394.
[15] B.N.N. Achar, G.W. Brindley and J.H. Sharp, Proc. Int. Clay Conf., Jerusalem, 1 (1966) 67.
[16] J.K. Chen and T.B. Brill, Thermal decomposition of energetic materials 54. Kinetics and near-surface products of azide polymers AMMO, BAMO, and GAP in simulated combustion, Combustion and Flame, 87 (1991) 157–168.
[17] J.K. Chen and T.B. Brill, Chemistry and kinetics of hydroxyl-terminated polybutadiene (HTPB) and diisocyanate–HTPB polymers during slow decomposition and combustion-like conditions, Combustion and Flame, 87 (1991) 217–232.
[18] Du Tingfa, Thermal decomposition studies of solid propellant binder HTPB, Thermochim. Acta, 138 (1989) 189–197.
[19] S. Tamura and J.K. Gillham, Pyrolysis-molecular weight chromatography–vapor-phase infrared spectrophotometry: an on-line system for analysis of polymers. IV. Influence of cis/trans ratio on the thermal degradation of 1,4-polybutadienes, J. Appl. Polym. Sci., 22 (1978) 1867–1884.
[20] W.H. Andersen, K.W. Bills, E. Mishuck, G. Moe and R.D. Schultz, A model describing combustion of solid composite propellants containing ammonium nitrate, Combustion and Flame, 3 (1959) 301–317.